Characterization of Erbium and Ytterbium Co-doped TiO₂ Synthesized using the Sol-gel Process for Photon Up-conversion Applications

Viriya Laohakul[1], Kanokthip Boonyarattanakalin[1], Wanichaya Mekprasart[1] and Weerachon Phoohinkong[2],*

[1] *College of Materials Innovation and Technology, King Mongkut's Institute of Technology Ladkrabang, Bangkok, 10520, Thailand*

[2] *Faculty of Science and Technology, Suan Dusit University, Bangkok, 10700, Thailand*

Abstract

TiO₂-based up-conversion materials dually doped with $0.2\%Er^{3+}$ and $10/12\%Yb^{3+}$ were synthesized using the sol-gel method. The samples were subjected to a calcination process at 500°C for 2 hr. X-ray diffraction, scanning electron microscopy, UV-VIS diffuse reflectance spectroscopy, and X-Ray Photoelectron Spectroscopy were employed to investigate the effect of dopant concentration on the morphology, crystal structure, and up-conversion properties of the prepared samples. The results indicate that the prepared doped samples retained the anatase TiO₂ crystalline phase and did not show any significant difference in morphology. Moreover, the band gap energy of TiO₂ was found to decrease from the typical 3.2 eV (pristine TiO₂) to 3.17 and 3.03 eV for the $0.2\%Er^{3+}$ with 10 and $12\%Yb^{3+}$ dopants, respectively, which can be attributed to the presence of Yb*4f* valence edge states. The Er*4f* state exhibited a transition absorption state in the near-infrared light range, indicating its crucial role in the potential up-conversion mechanism of the prepared doped samples.

Keywords: Titanium dioxide, Rare-earth, Er-Yb doping, Up-conversion, Sol-gel

1. Introduction

Extensive research has been conducted to enhance the efficiency of photocatalyst materials for various applications in the fields of energy and environment. Among the most widely investigated photocatalytic materials is Titanium dioxide (TiO₂), known for its high photoactivity and excellent chemical and physical stability. The photocatalytic properties of TiO₂ are influenced by several factors, including surface structure and electronic structure. The electronic structure is also related to the crystal structure and impurity atoms, and vice versa. Titanium dioxide typically exists in three main phases: anatase, rutile, and brookite. The anatase phase exhibits high photocatalytic efficiency, while the rutile phase possesses a more favorable band gap structure and superior chemical stability, albeit with lower photocatalytic activity [1]-[3]. When titanium dioxide is exposed to light energy exceeding its band gap energy, the electron (e⁻) absorbs energy and transitions from the valence band state to the conduction band state, leading to the formation of high-energy electron-hole pairs and generating corresponding high-energy radicals. This process serves as a crucial mechanism for photocatalysis [3]-[5]. However, the practical application of titanium dioxide faces certain limitations when exposed to sunlight. Firstly, the recombination rate of electrons and holes is high, which hinders efficient charge separation. Secondly, TiO₂ is a wide band gap semiconductor with an energy gap of approximately 3.2 eV, necessitating high-energy ultraviolet (UV) light for effective electron-hole pair generation.

Corresponding Author : weerachon_pho@dusit.ac.th

As a result, the photocatalytic efficiency of TiO_2 under sunlight is relatively low. In light of these limitations, extensive research has been undertaken to enhance the efficiency of titanium dioxide photocatalysis under sunlight to harvest more light energy within the visible and infrared frequency ranges, where a significant portion of solar radiation resides.

In recent years, the incorporation of rare earth (RE) metals doped into TiO_2 structure has emerged as an effective approach to enhance the photocatalytic properties of TiO_2. This doping strategy offers several advantages, including the modification of the band-gap energy structure to enable the utilization of visible light energy, the improvement of the electronics structure within the infrared energy range for up-conversion to higher energy levels, and the enhancement of the surface structure by utilizing the active sites provided by the rare earth f-orbitals for substrate absorption onto the TiO_2 surface. The incorporation of $4f$ electron shell states plays a crucial role in enhancing the electronic structure, facilitating the absorption of low-energy photons to the excited state and facilitating the transition to lower-energy states that can emit high-energy photons through various mechanisms, including excited-state absorption and cross-relaxation. This energy transfer upconversion phenomenon is particularly significant in TiO_2 particles doped with Er and Yb, as it enables the conversion of lower-energy photons into higher-energy ones, thereby expanding the range of light that can be effectively utilized by the photocatalytic system. The incorporation of Yb^{3+} doped in TiO_2 particles introduces an absorption range centered around 980 nm. The presence of Yb^{3+} and Er^{3+} absorption state enhances the infrared absorption capabilities and facilitates efficient excitation energy transfer from Yb^{3+} to Er^{3+}. Consequently, the Yb^{3+}-Er^{3+} couple dope system exhibits remarkable efficiency in the upconversion process. Moreover, the TiO_2 up-conversion materials have gained significant attention for various applications, particularly in the field of photocatalysis for pollutant degradation [5]. Furthermore, this hybrid system has demonstrated potential utilization in diverse fields such as light-triggered drug delivery in pharmaceuticals [6], light amplification in biosensors [7], light-driven water splitting [8], [9], and solar energy harvesting technology [5], [10], [11].

Joanna Reszczynska *et al.* [12] investigated the photocatalytic activity of titania-based materials doped with rare earth metals (Er^{3+}, Yb^{3+}, or Er^{3+}/Yb^{3+}). The sol-gel method was employed to prepare visible light-activated anatase systems with varying concentrations of lanthanide precursors (ranging from 0.25 to 10 mol%). Among the tested samples, Yb^{3+}-TiO_2, specifically containing 1 mol% ytterbium, exhibited the highest photocatalytic activity under visible light irradiation (>450 nm). Notably, the presence of high concentrations of Yb or Er alone negatively impacted the photocatalytic performance, whereas the Yb^{3+}-Er^{3+} pairs, particularly at concentrations of 0.25Er and 0.5Yb, demonstrated the best results, while 2Er and 10Yb showed the poorest performance. This study focuses on the synthesis and analysis of the Yb^{3+}-Er^{3+} couple-doped up-conversion system via the sol-gel method. Specifically, we investigate the optical properties and structural characteristics of TiO_2 doped with 0.2% Er and varying Yb concentrations of 10% and 12%. This concentration range is particularly interesting as it represents an unexplored gap in the literature. Based on the research findings of Bhethanabotla, Russell, & Kuhn [13], it has been observed that a higher percentage of Yb is crucial for the generation of electron-hole pairs. Consequently, an intriguing aspect emerges wherein the Yb ratio is relatively higher while the Er ratio is comparatively lower. This observation highlights the potential significance of optimizing the Yb content in relation to Er in order to enhance the desired electron-hole pair formation. We aim to provide a more comprehensive understanding of the Yb^{3+}-Er^{3+} couple-doped TiO_2 up-conversion system, thereby contributing to the improvement of synthesis techniques for its utilization in various applications.

2. Experimental

2.1 Materials

Analytical reagent grade titanium(IV) isopropoxide (TTIP) was obtained from Sigma-Aldrich. It served as the titanium precursor for TiO_2 synthesis. Ytterbium(III) nitrate pentahydrate $(Yb(NO_3)_3 \cdot 5H_2O)$ and erbium(III) nitrate pentahydrate $(Er(NO_3)_3 \cdot 5H_2O)$ were analytical reagent grade, purchased from Sigma–Aldrich, was employed as the rare-earth dopant source. Commercially available TiO_2 P25 nanoparticles were procured from Ajax Finechem Pty. Ltd. and were used as reference material. Ethanol and ammonia were used as received from Merck. Deionized water was employed for all reaction processes.

2.2 Preparation details

Er-Yb dually doped TiO_2 was synthesized using the sol-gel method. In a typical procedure, erbium(III) nitrate pentahydrate and ytterbium(III) nitrate pentahydrate were dissolved in deionized water in specific ratios of 0.2:10% and 0.2:12%. The resulting solutions were adjusted to a volume of 50 mL under continuous vigorous agitation. Separately, a solution of 50 mL 0.25 M TTIP in 99.9% ethanol was prepared and added to the metal salt solutions, followed by stirring until an opaque sol was formed. The pH of the solution was adjusted to the range of 5-6 using the dropwise addition of ammonia solution. The resulting transparent solution was further stirred for an additional hour until clarity was achieved. The obtained gel was washed with deionized water and subsequently dried at 100°C for 24 hours in an oven. The dried gel was ground to obtain a powder form, which was then calcined at 500°C for 2 hours.

2.3 Characterizations

X-ray diffraction analysis was performed to determine the crystalline phase of the sample in the 2θ range of 10-90° using a Rigaku model SmartLab X-ray diffractometer with Cu target Kα-ray (λ = 1.5404 Å). HITACHI Scanning electron microscopy model SU6600 was used to examine morphology. UV-VIS diffraction reflectance spectroscopy, and DRS of Perkin Elmer model LAMBDA 750s spectrophotometer were performed to study the absorption and reflectance behavior in the UV and visible regions employed to analyze the optical properties and band gap energy of the TiO_2. X-ray Photoelectron Spectroscopy, XPS of JEOL model JPL-9010MC was used at survey scan and core level high-resolution scan to investigate the chemical composition and surface states.

3. Results and discussion

3.1 Scanning electron microscopy (SEM)

Fig. 1, the SEM image of the titanium dioxide (TiO_2) up-conversion materials reveals that they exhibit similar morphological characteristics, suggesting that the Yb dopant ratio does not significantly influence the morphology. The resultant particles exhibit an irregular square shape with particle sizes ranging from 13 to 100 micrometers. The SEM-EDS (Energy Dispersive Spectroscopy) spectra reveal the presence of Yb in both TiO_2 samples, while the signal of Er is not detected. This absence of Er signal can be attributed to the possibility of a low concentration of Er or Er doping within the TiO_2 lattice or particles.
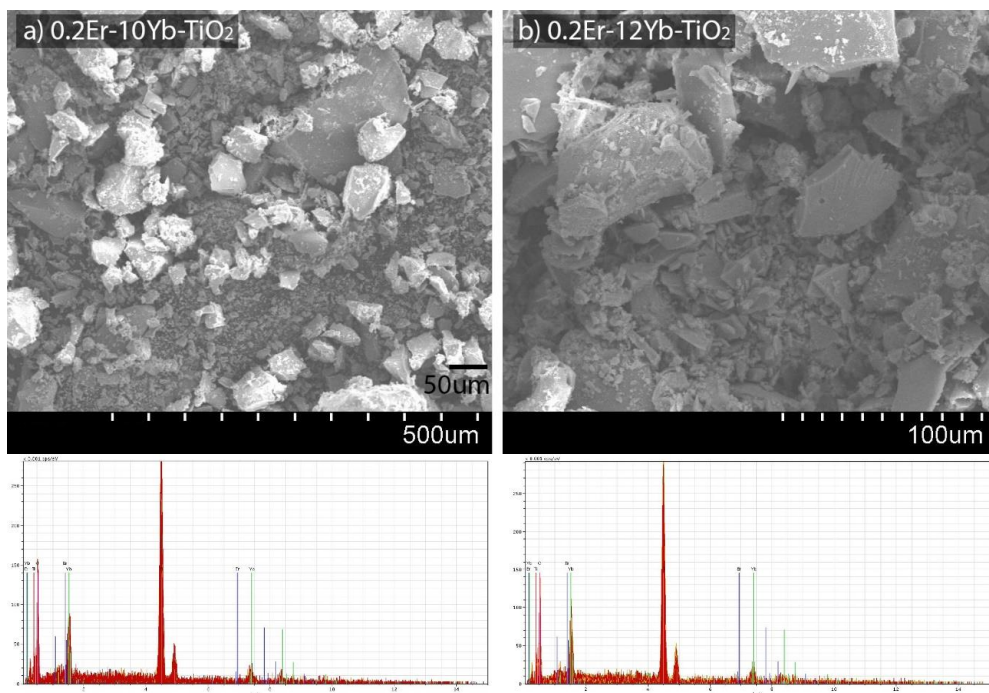
Fig. 1. Amorphous structural characteristics of titanium dioxide upconversion material doped 0.2 erbium at 10 and 12% ytterbium of a) 0.2Er-10Yb-TiO$_2$ and b) 0.2Er-12Yb-TiO$_2$

3.2 X-ray diffraction

Fig. 2. illustrates the X-ray diffraction pattern of the titanium dioxide-doped upconversion materials, the 0.2Er-10Yb-TiO$_2$ and 0.2Er-12Yb-TiO$_2$ samples. The diffraction pattern exhibits prominent peaks at 25.2º, 37.8º, 48.0º, 54.8º, 62.7º, and 75.4º, which correspond to the crystallographic planes (101), (004), (200), (105), (204), and (215) of the anatase phase of titanium dioxide, respectively [14]. No significant diffraction peaks corresponding to unreacted ytterbium or erbium oxides were observed, which may be indicating their successful incorporation into the titanium dioxide lattice. It can be inferred that the doping process does not adversely affect the crystal structure of titanium dioxide. The sol-gel synthesis method employed in this study enables the synthesis of titanium dioxide with a pure anatase crystalline phase. Which well-known that the anatase TiO$_2$ phase possesses favorable reactivity and facilitates the generation of efficient photoactive electron-hole pairs [14], [15]. Moreover, the larger atomic radii of Er^{3+} and Yb^{3+} compared to that of Ti atom can lead to alterations in the crystalline structure and crystallinity of TiO$_2$ when these dopants replace Ti atoms. The atomic radius of Er is approximately 176 picometers (pm), while Yb has a similar atomic radius of around 176 pm. These values are larger than the atomic radius of titanium, which is approximately 147 pm. The incorporation of Er and Yb ions into the TiO$_2$ lattice with their larger atomic sizes can result in lattice expansion and a subsequent mismatch in the TiO$_2$ lattice structure. This expansion occurs due to the substitution of smaller Ti ions by larger Er and Yb ions, which disrupts the regular arrangement of the TiO$_2$ lattice and introduces strain and lattice distortion. This substitution induces a notable shift towards a more amorphous, particularly with a significant increase observed at 12% Yb in 0.2% Er condition. This also corresponds to the results of Er and Yb doping in TiO$_2$ at other concentrations [12].
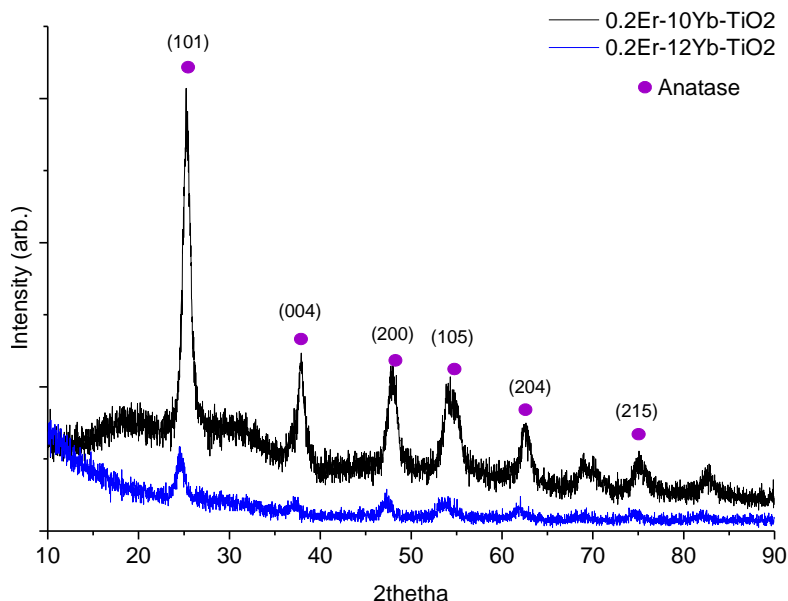
Fig. 2. X-ray diffraction patterns of titanium dioxide upconversion material doped 0.2 erbium at 10 and 12% ytterbium of 0.2Er-10Yb-TiO$_2$ and 0.2Er-12Yb-TiO$_2$

3.3 X-ray Photoelectron Spectroscopy (XPS) study

XPS survey spectra of the 0.2Er-10Yb-TiO$_2$ and 0.2Er-12Yb-TiO$_2$ samples are in Fig.3. a) and b) shows the overall comprehensive analysis of trace elements and chemical compositions on the sample's surface. The main peaks observed in the survey spectra are attributed to the O*1s* and Ti*2p* signals, which correspond to the predominant composition of TiO$_2$ in the host material. The presence of trace elements of Yb^{3+} is confirmed by their distinct signals detected on both sample surfaces. However, the absence of a significant Er^{3+} signal suggests either a low concentration of Er^{3+} or Er^{3+} doping within the TiO$_2$ lattice or particles, which aligns with the findings of the SEM-EDS analysis. The presence of C*1s* signals can be attributed to adsorbed carbon, which is used to adjust the binding energy shift at 284.8 eV, which corresponds to carbon in C-C and C-H environments. The insets in panels (a) and (b) provide a close inspection and detailed examination of the valence electronic structure, enabling differentiation from XPS survey spectra of general TiO$_2$ [3], [16]. Typically, TiO$_2$ XPS spectra predominantly exhibit the Ti*3s* and Ti*3p* states at approximately 62 eV and 36-38 eV, respectively, along with a minor contribution from the O*2s* state around 22 eV. The valence density, ranging from 0-10 eV, is usually very small due to the combination of O*2p* with minor Ti*4s* and negligible Ti*3d* states composition [3], [17]-[19]. In contrast, the prominent valence peak edge observed around 0-10 eV in the samples indicates the contribution of the Yb*4f* state, which is further supported by the corresponding weak signal of the Yb*5p* state at approximately 26 eV. This confirms the presence of Yb^{3+} in the samples. The confirmation of the presence of Yb^{3+} in the samples is further supported by the well agree with the valence edge electronic peak shape reported form by Nemoshkalenko *et al.* [20].

The core level Ti*2p* XPS features of the 0.2Er-10Yb-TiO$_2$ and 0.2Er-12Yb-TiO$_2$ samples, as depicted in Figure 3(c) and (d), exhibit doublet peaks arising from the spin-orbit splitting of Ti*2p$_{3/2}$* and Ti*2p$_{1/2}$*, which the peak positions at 458.3 and 458.6 eV, respectively, indicate that the Ti*2p$_{3/2}$* peak corresponds to the main of intrinsic Ti^{4+} state on the TiO$_2$ surface.
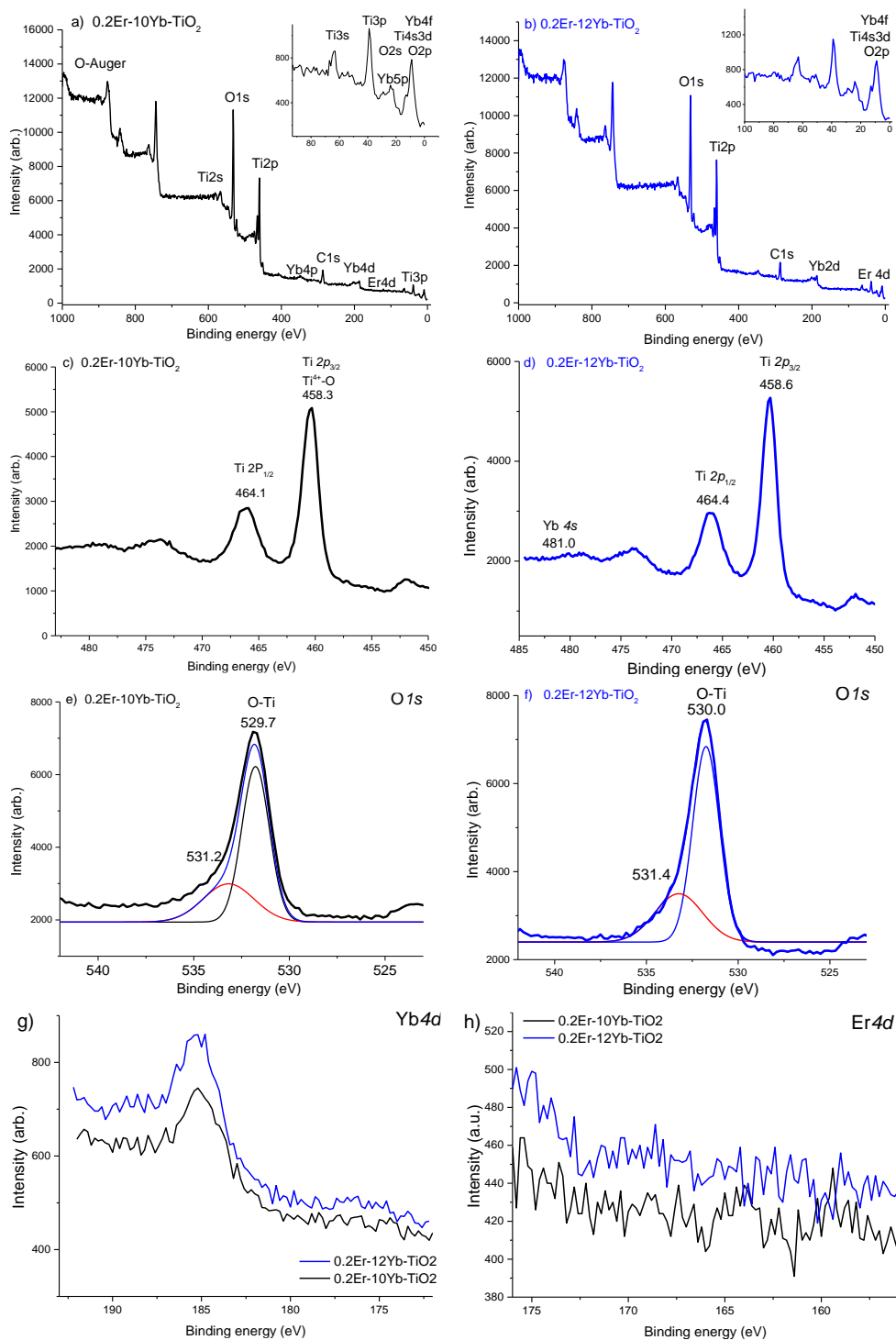
Fig. 3. XPS spectra of 0.2Er-10Yb-TiO$_2$ and 0.2Er-12Yb-TiO$_2$: a) and b) survey spectra, c) and d) high resolution XPS spectra of Ti*2p*, e) and f) of O*1s*, g) of Yb*4d*, and h) of Er*4d* regions

This observation is consistent with the main TiO_2 anatase phase identified through XRD analysis. The structural characteristics of the Er-Yb doped TiO_2 system typically align with the anatase structure of TiO_2, in agreement with the reported in the different synthesis methods in literature [21]. However, a slight shift in the binding energy of the Ti$2p_{3/2}$ peak towards a lower-than-typical bare TiO_2 system was also able to be observed, even though this is not prominently observed in the Er-Yb doped system. This deviation may be attributed to the generation of a small component of Ti^{3+} defect states induced by the presence of Er and Yb dopants in the TiO_2 host lattice [22]-[24]. The Ti$2p_{3/2}$ peak of 0.2Er-10Yb-TiO_2, located at 458.3 eV, exhibits a lower binding energy compared to 0.2Er-12Yb-TiO_2, despite the latter having lower crystallinity. This discrepancy is likely attributed to a higher doping degree in the 0.2Er-12Yb-TiO_2 sample. With an increase in Yb dopant concentration, may be ascribed that the TiO_2 crystals experience a reduction in crystallization due to the higher doping level. Consequently, TiO_2 separates into smaller crystalline domains with lower incorporation of dopant atoms within the host lattice. This phenomenon leads to an increase in the binding energy shift towards 458.6 eV, approaching the binding energy of bare TiO_2. The high-resolution XPS spectra of the O$1s$ level peaks in the 0.2Er-10Yb-TiO_2 and 0.2Er-12Yb-TiO_2 samples were subjected to deconvolution, resulting in two distinct peaks (Fig.3. e) and f)). The peak centered at lower binding energy corresponds to the lattice oxygen of TiO_2, while the peak centered at higher binding energy can be attributed to the presence of adsorbed hydroxyl oxygen on the surface. A slight shift in the binding energy of the O$1s$ peak is observed, which correlates with the slight shift observed in the Ti$2p$ level peak. This shift is commonly observed in Er and Yb-doped TiO_2 systems [22], [25], [26], where the O$1s$ binding energy is shifted towards lower values compared to bare TiO_2. This shift is likely a result of the Er-O and/or Yb-O environment. Conversely, the presence of O_v induces a slight shift towards higher binding energy [27]. The observed results may be attributed to the low concentration of doping in the TiO_2 system. The XPS binding energy curves shown in Fig. 3. g) and h), provide insight into the Yb$4d$ and Er$4d$ regions, respectively. The analysis reveals the presence of Yb at the surface of the particles in both samples, whereas Er is not observed. This finding confirms the presence of Yb in the samples, while suggesting that Er may be present in very low concentrations compared to Yb and/or incorporated inside the particle, thereby explaining its absence at the surface. XPS binding energy curves of Fig.3. g) and h) at Yb$4d$ and Er$4d$ regions indicated that small intensities of Yb were observed without Er at the surface particles in both samples. This result confirmed Yb in sample while Er could not appear at the surface, however, may be due to the very low concentration compared to the Yb.
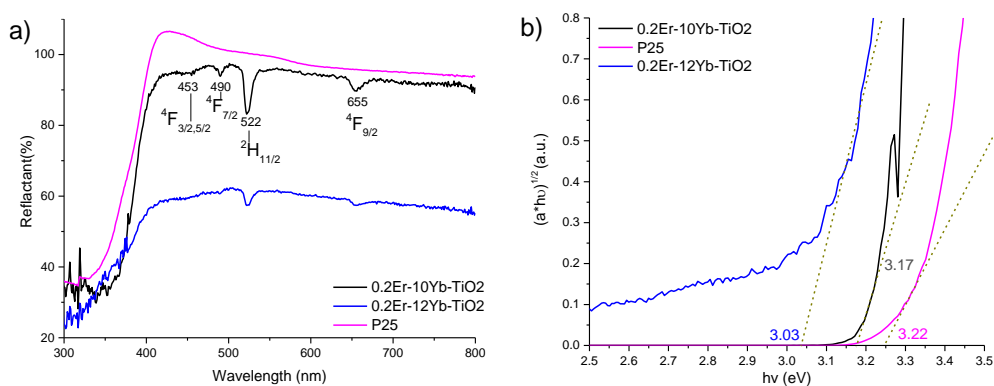

Fig. 4. UV–vis DRS spectra a) and the corresponding Kubelka-Munk absorption energy b) of 0.2Er-10Yb-TiO_2 and 0.2Er-12Yb-TiO_2 compared with standard P25-TiO_2

3.4 Optical properties

The UV–vis diffuse reflectance spectra presented in Fig. 4. a), were compared with P25-TiO_2 used as the reference sample. It is observed that all the doped samples exhibit strong absorption below 380 nm, which is an O$2p$ transition to Ti$3d$ state characteristic feature of pristine TiO_2. Notably, the doped samples display a slight shift of their absorption edge towards the visible light region when compared to P25-TiO_2 (absorption band edge around 390 nm, band gap 3.2 eV) and shift higher along with Yb dopant concentration increase at 12%Yb, or the other hand is a shift toward lower band gap energy compared to P25-TiO_2 as show the Kubelka-Munk absorption energy plot in Fig. 4. b). The band gap energy of the 0.2Er-10Yb-TiO_2, 0.2Er-12Yb-TiO_2, and standard P25-TiO_2 were 3.17, 3.03, and 3.22 eV, respectively. The observed lower band gap energy, as indicated by the XPS results, can be attributed to the combined effect of the high density of Yb$4f$ state at the valence band edge of TiO_2 host. This reduced the gap energy and enhanced the transition probability to the conduction band state, which Ti$3d$ is the main composition, as supported by the calculated DOS structure reported by Nemoshkalenko *et al.* [20]. The influence of surface defect states stemming from amorphousity was not taken into account, as no significant surface Ti^{3+} and O_v states were detected. This observation trend is consistent with previous findings reported by Reszczyńska *et al.* in a different Er and Yb concentration doped system [12]. Furthermore, it is evident that distinct absorption peaks are observed at 453 nm, 490 nm, 522 nm, and 655 nm. These peaks can be attributed to the transitions to Er^{3+}, of $^4F_{3/2,5/2}$, $^4F_{7/2}$, $^2H_{11/2}$, and $^4F_{9/2}$ excited states from the $^4I_{15/2}$ ground state [12], [13], [25], [28] as depicted in Fig. 4. a) which are associated with the up-conversion transition mechanism. The energy differences associated with these transitions are slightly different from those reported by Reszczyńska *et al.* This result serves as clear confirmation of the presence of Er^{3+} in both TiO_2 samples. The up-conversion mechanism Er and Yb co-doped TiO_2 involves the intra Yb$4f$ and Er$4f$ electronic structures and inter-electron transfer through Yb$^2F_{5/2}$ sensitized Er$4f$. This process promotes the emission of higher energy photons during the Er$4f$ to ground state transition, particularly in the transitions of Er^{3+} $^4F_{3/2} \rightarrow {}^4I_{15/2}$, $^4F_{7/2} \rightarrow {}^4I_{15/2}$, $^2H_{11/2} \rightarrow {}^4I_{15/2}$, and $^4F_{9/2} \rightarrow {}^4I_{15/2}$. These transitions are significant components of the up-conversion mechanism. The presence of these Er$4f$ states provides evidence for the existence of other Er$4f$ states, including the $^4S_{3/2} \rightarrow {}^4I_{15/2}$ transition and the higher energy photon emission during the $^2G_{11/2} \rightarrow {}^4I_{15/2}$ transition. These additional Er$4f$ states play a crucial role in the overall up-conversion mechanism.

4. Conclusion

TiO_2 particles doped with 0.2% Erbium at 10% and 12% Ytterbium were successfully synthesized using the sol-gel method. The incorporation of Yb in the TiO_2 host has been confirmed through SEM-EDS and XRD analysis, while the presence of Er was confirmed through optical properties analysis. The synthesized Er-Yb dually doped TiO_2 upconversion material exhibited a retained anatase TiO_2 crystalline structure, with differences in crystallinity, slight differences in surface defects state, titanium valence state, and oxygen vacancy, while no significant variations in morphology were observed. The obtained Er-Yb dually doped TiO_2 upconversion material displayed improved absorption in the visible light region and near-infrared light due to the Er$4f$ state transition. This transition played a crucial role in the up-conversion mechanism.

Acknowledgment

References

[1] De Angelis F, Di Valentin C, Fantacci S, Vittadini A, Selloni A. Theoretical studies on anatase and less common TiO_2 phases: bulk, surfaces, and nanomaterials. Chem. Rev. 2014;114(19):9708-53.

[2] Bourikas K, Kordulis C, Lycourghiotis A. Titanium dioxide (anatase and rutile): surface chemistry, liquid-solid interface chemistry, and scientific synthesis of supported catalysts. Chem. Rev. 2014;114(19):9754-823.

[3] Kapilashrami M, Zhang Y, Liu Y-S, Hagfeldt A, Guo J. Probing the optical property and electronic structure of TiO_2 nanomaterials for renewable energy applications. Chem. Rev. 2014;114(19):9662-707.

[4] Nosaka Y, Nosaka AY. Generation and detection of reactive oxygen species in photocatalysis. Chem. Rev. 2017;117(17):11302-36.

[5] Yang X, Wang D. Photocatalysis: from fundamental principles to materials and applications. ACS Appl. Energy Mater. 2018;1(12):6657-93.

[6] Zhao J, Xu J, Jian X, Xu J, Gao Z, Song Y-Y. NIR light-driven photocatalysis on amphiphilic TiO_2 nanotubes for controllable drug release. ACS Appl. Mater. Interfaces 2020;12(20):23606-16.

[7] Qiu Z, Shu J, Tang D. $NaYF_4$:Yb,Er upconversion nanotransducer with in situ fabrication of Ag_2S for near-infrared light responsive photoelectrochemical biosensor. Anal. Chem. 2018;90(20):12214-20.

[8] Wang Q, Domen K. Particulate photocatalysts for light-driven water splitting: mechanisms, challenges, and design strategies. Chem. Rev. 2020;120(2):919-85.

[9] Maeda K. Z-Scheme Water splitting using two different semiconductor photocatalysts. ACS Catal. 2013;3(7):1486-503.

[10] Li K, Peng B, Peng T. Recent advances in heterogeneous photocatalytic CO_2 conversion to solar fuels. ACS Catal. 2016;6(11):7485-527.

[11] Ma Y, Wang X, Jia Y, Chen X, Han H, Li C. Titanium dioxide-based nanomaterials for photocatalytic fuel generations. Chem. Rev. 2014;114(19):9987-10043.

[12] Reszczyńska J, Grzyb T, Sobczak JW, Lisowski W, Gazda M, Ohtani B, *et al.* Visible light activity of rare earth metal doped (Er^{3+}, Yb^{3+} or Er^{3+}/Yb^{3+}) titania photocatalysts. Appl. Catal., B Environ. 2015;163:40-9.

[13] Bhethanabotla VC, Russell DR, Kuhn JN. Assessment of mechanisms for enhanced performance of Yb/Er/titania photocatalysts for organic degradation: Role of rare earth elements in the titania phase. Appl. Catal., B Environ. 2017;202:156-64.

[14] Challagulla S, Tarafder K, Ganesan R, Roy S. Structure sensitive photocatalytic reduction of nitroarenes over TiO_2. Sci. Rep. 2017;7(1):8783.

[15] Buchalska M, Kobielusz M, Matuszek A, Pacia M, Wojtyła S, Macyk W. On oxygen Activation at Rutile- and Anatase-TiO_2. ACS Catal. 2015;5(12):7424-31.

[16] Junkar I, Kulkarni M, Benčina M, Kovač J, Mrak-Poljšak K, Lakota K, *et al.* Titanium dioxide nanotube arrays for cardiovascular stent applications. ACS Omega 2020;5(13): 7280-9.

[17] Vázquez-López A, Maestre D, Martínez-Casado R, Ramírez-Castellanos J, Píš I, Nappini S, *et al.* Unravelling the role of lithium and nickel doping on the defect structure and phase transition of anatase TiO_2 nanoparticles. J. Mater. Sci. 2022;57(14):7191-207.

[18] Xu T, Wu H, Cui K, Zhao Q, Huang J, Wei L, *et al.* Hybrid TiO_2/WO_3 nanoparticles fabricated via a sol-gel process using amphiphlic poly(ε-caprolactone)-block-poly(acrylic acid) diblock copolymer as template and their high visible light photocatalytic activity. SN Appl. Sci. 2019;1(8):866.

[19] Zatsepin DA, Boukhvalov DW, Gavrilov NV, Zatsepin AF, Shur VY, Esin AA, *et al.* Soft electronic structure modulation of surface (thin-film) and bulk (ceramics) morphologies of TiO_2-host by Pb-implantation: XPS-and-DFT characterization. Appl. Surf. Sci. 2017;400:110-7.

[20] Nemoshkalenko VV, Borisenko SV, Uvarov VN, Yaresko AN, Vakhney AG, Senkevich AI, *et al.* Electronic structure of the $R_2Ti_2O_7$ (R=Sm–Er, Yb, Lu) oxides. Phys. Rev. B 2001;63(7):075106.

[21] Yildirim S, Yurddaskal M, Dikici T, Aritman I, Ertekin K, Celik E. Structural and luminescence properties of undoped, Nd^{3+} and Er^{3+} doped TiO_2 nanoparticles synthesized by flame spray pyrolysis method. Ceram. Int. 2016;42(9):10579-86.

[22] Trabelsi F, Mercier F, Blanquet E, Crisci A, Salhi R. Synthesis of upconversion TiO_2:Er^{3+}-Yb^{3+} nanoparticles and deposition of thin films by spin coating technique. Ceram. Int. 2020;46(18, Part A):28183-92.

[23] Rao Z, Xie X, Wang X, Mahmood A, Tong S, Ge M, *et al.* Defect Chemistry of Er^{3+}-Doped TiO_2 and Its Photocatalytic Activity for the Degradation of Flowing Gas-Phase VOCs. J. Phys. Chem. C 2019;123(19):12321-34.

[24] Jiang X, Li C, Liu S, Zhang F, You F, Yao C. The synthesis and characterization of ytterbium-doped TiO_2 hollow spheres with enhanced visible-light photocatalytic activity. RSC Advances. 2017;7(40):24598-606.

[25] Mazierski P, Roy JK, Mikolajczyk A, Wyrzykowska E, Grzyb T, Caicedo PNA, *et al.* Systematic and detailed examination of $NaYF_4$-Er-Yb-TiO_2 photocatalytic activity under Vis–NIR irradiation: Experimental and theoretical analyses. Appl. Surf. Sci. 2021;536:147805.

[26] Chen F-H, Her J-L, Shao Y-H, Matsuda YH, Pan T-M. Structural and electrical characteristics of high-κ Er_2O_3 and Er_2TiO_5 gate dielectrics for a-IGZO thin-film transistors. Nanoscale Res. Lett. 2013;8(1):18.

[27] Phoohinkong W, Pavasupree S, Mekprasart W, Pecharapa W. Synthesis of low-cost titanium dioxide-based heterojunction nanocomposite from natural ilmenite and leucoxene for electrochemical energy storage application. Curr. Appl Phys. 2018;18:S44-S54.

[28] Zheng Y, Wang W. Electrospun nanofibers of Er^{3+}-doped TiO_2 with photocatalytic activity beyond the absorption edge. J. Solid State Chem. 2014;210(1):206-12.